

Application of Variational Asymptotic Method for Structural Analysis of Fan Rotor Blades in Boundary Layer Ingesting Flow Field

Mohit Gupta*

University of Colorado, Boulder, CO 80309

Manish Pokhrel[†], Dewey H. Hodges[‡]*, and Dimitri N. Mavris[§]

Georgia Institute of Technology, Atlanta, Georgia, 30332

Boundary Layer Ingestion (BLI) appears to be a promising technology for reducing aircraft fuel burn. Despite potential benefits, there are several challenges associated with BLI. A primary concern is the structural integrity of the fan blades experiencing unsteady forces due to unequal work input from the rotor at different circumferential locations of the engine annulus. In the conceptual design phase, rapid turnaround is as important as measuring the stresses accurately. Through the present work, the authors present a computationally efficient framework for measuring natural frequencies and analyzing time histories of 3-D stresses in nonlinear transient structural analyses of rotating fan blades. This framework uses state of the art tools developed for beam modeling based on Variational Asymptotic Method and the Geometrically Exact Beam Theory. The authors also provide verification of the present framework against 3-D finite element analysis performed in COMSOL.

I. Introduction

Various tightly integrated aircraft concepts have emerged as a result of aggressive performance goals set forth by various organizations. One technology common in most integrated aircraft systems is the concept of Boundary Layer Ingestion (BLI). BLI is a concept in which a set of propulsors on a vehicle ingest a portion of that vehicle's viscous boundary layer. The result is typically that the propulsive efficiency of the device is improved, thereby reducing fuel burn. As such, it is necessary to quantify these impacts during the conceptual design phase to assess various concepts. However, a number of significant challenges - both on modeling and design - appear as a result of BLI. Various studies [1–4] have been conducted to capture the impacts of BLI on the the propulsion system, such as those in the inlet, fan, and nozzle. Many BLI propulsor modeling studies use representative fan maps and scale them accordingly. Sometimes, a small drop in efficiency is assumed to model BLI losses. However, intuition tells us that instead of using conventional maps, we need to first design a fan for BLI and generate corresponding maps as the operating conditions are inherently different for BLI fans.

While maximizing aerodynamic performance of the fan is the objective function, the mechanical integrity is a constraint. Major mechanical concerns associated with fans ingesting distorted flow are large resonant fan blade response and vibratory stresses during rotation. As the blades rotate in a distorted flow field, the flow on the blade changes at each circumferential location. The unsteady pressure loading on each blade acts as an external forcing on the blade. The stresses on the blades will be oscillatory - with a mean stress and some alternating stress. In the study done under the BLI2DTF group [5], it was found that the reference fan (fan for under-wing engine applications) was not able to satisfy the Goodman requirement. Currently, conceptual design framework for fan designs do not account for dynamic analysis of fan blades. In order to develop the framework, a key enabler is to be able to analyze the rotor blade structure subjected to periodic forces in a computationally efficient manner.

Structural analysis comprises of evaluating the behavior of a component (or a combination of components) under a set of prescribed conditions. This is a major step in ensuring the mechanical integrity of the component under consideration. For any kind of structural analysis, the loads, geometry, boundary condition, and mechanical properties

*Postdoctoral Associate, Mechanical Engineering, AIAA Member

[†]Senior Graduate Researcher, ASDL, Daniel Guggenheim School of Aerospace Engineering, AIAA Student Member

[‡]Professor, Daniel Guggenheim School of Aerospace Engineering, AIAA Fellow

[§]S.P. Langley Distinguished Regents Professor and Director of ASDL, Daniel Guggenheim School of Aerospace Engineering, AIAA Fellow

of the material needs to be known. The outcome of such analysis typically includes stresses, strains, and displacements. These parameters are then compared to the failure criteria for the material. For static analysis, the loads are invariant with time. For BLI like analysis, however, the loads vary with time, so the dynamic response of the blade needs to be examined. In the present work, we perform the structural analysis of fan blades that are beam like structures as they have one dimension much longer than the other two dimensions but include a large amount of twist and other geometrical intricacies which are characteristic to the blades. Fundamental theories and techniques of elasticity can be used to solve the beam-like structures. Although computationally fast, these theories do not yield satisfactory results. 3-D Finite Element Method (FEM) is considered to be better suited for analysis of composite materials and complex geometries. Finite Element Method numerically solves the partial differential equations derived from the fundamental theories of mechanics. Although the results are mostly satisfactory in terms of accuracy, the computational expense of these 3-D FEM models is much higher (more than an order of magnitude) compared to beam models. What's more is that creating 3-D models of these complex geometries for FEM analysis can also be extremely time consuming.

II. Fan Blade Structural Analysis for BLI

In cases of embedded engines, the severity of flow distortion needs to be accounted for in almost all mission conditions. If the dynamic stresses resulting from the interactions of the flow and the rotor are not addressed, then the structure might be prone to failure. Therefore, in the conceptual design phase, where rapid turnaround is a requirement, numerical modeling of this integrated aero-mechanical problem becomes a challenge in a sense that both computational efficiency and accuracy needs to be present. The goal is to achieve a certain margin in the Goodman diagram and the Campbell diagram.

The equations governing the dynamics of the blade structure are used to calculate the vibratory and mean stresses at the forces induced by unequal pressure rise on the flow. The formulation for structural analysis involving the Variational Asymptotic Method (VAM) as described in Sec. III includes calculations of natural frequencies. When the natural frequency of the blades come close to these forced excitation frequencies, resonant response is expected. The use of Campbell diagram is made to analyze the margin between the natural frequency at a given mode of vibration and the excitation frequency on the blade at a given distorted inflow and RPM.

Figure 1 shows a Campbell diagram that can be used to explain its application. The horizontal axis is the speed of rotation and the vertical axis is the frequency. The lines passing through origin are the excitation frequency lines and the curves (almost horizontal lines) are the natural frequencies at different nodes. At the speeds that the blades operate, if any of these two curves cross each other at any point, then resonance is likely to happen at that operating condition. A typical design practice is to ensure a 10% margin on resonance.

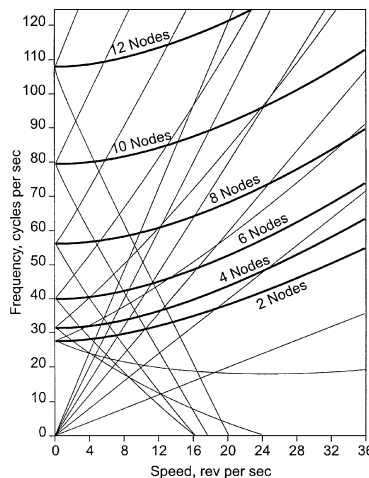


Fig. 1 Notional Campbell Diagram [6].

The stresses on the blades will be oscillatory - with a mean stress and some alternating stress. It is necessary to analyze the pair and determine whether it is in the material's operating limit. The steady stress may be well below the tensile stress of the material, but the alternating stresses present may cause the fan to operate outside the envelope

allowed for safe operation for a large number of cycles. A simple way of representing this envelope is with the help of a Goodman diagram (sometimes called a Haigh diagram) that draws the envelope of when the material fails. Figure 2 shows a sketch of a Goodman diagram, where the horizontal axis represents the mean stress and the vertical axis represents the alternating stress. Loosely speaking, the line joining the endurance limit (vertical axis) and ultimate tensile stress (horizontal axis) forms the Goodman line. Anywhere inside the region bounded by the Goodman line, the abscissa, and the ordinate, the blade can safely operate for a large number of cycles. In the following section (Section III), Variational Asymptotic Method (VAM) will be summarized briefly.

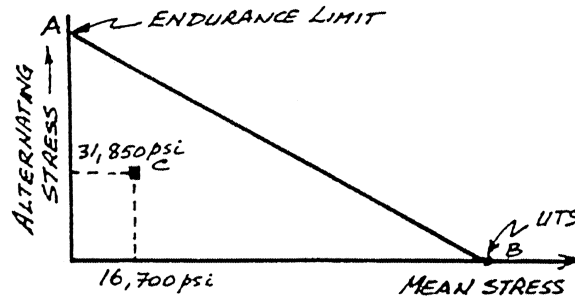


Fig. 2 Goodman diagram for blade stresses [7].

III. Variational Asymptotic Method

With the motivation of developing a fast and user-friendly method for analysis of complex aerospace structures, Variational Asymptotic Method (VAM) was employed for the first time almost 30 years back by Hodges et al. to perform structural analysis. With VAM, computational time is reduced by multiple orders of magnitude. One may argue that the 90s were actually the times to focus on developing tools which were fast because the computers were slow, bulky, and expensive. The advent of clever ways of manufacturing integrated circuits has led to a significant reduction in the cost of computation since then. With the developments in computer architecture, there is a reduction in the size of electronic components as well. This is an interpretation of Moore's law. But Moore's law, which primarily says that the cost of computing will decrease as we go forward in time, is now dead. The empirical data which is the basis of this law, itself shows that and it is confirmed by researchers at MIT and Intel. We can no longer count on computers getting faster and cheaper. Thus, developing and using the tools based on reduced-dimensional modeling remains a priority as they are fast, accurate, reliable as well as computationally efficient.

Hence, unlike many existing models, beam theories, and commercially available 3-D FEM tools for analyzing complex structures, the use of the Variational Asymptotic Method (VAM) [8] is proposed. It allows for a beam-like formulation that is free of ad-hoc assumptions. This is a synergistic approach where the computationally inexpensive nature of beam modeling using the VAM is combined with modeling procedures using sectional finite elements to obtain reliable models for high-fidelity, multi-physics simulations. The process of VAM involves deriving the 3-D equations in terms of cross-sectional 2-D constitutive relations and a set of geometrically exact one dimensional beam equation [9]. The one dimensional beam equations are solved and the 1-D stresses and strains are recovered into 3-D fields using the recovery relations developed from 2-D analysis. For detailed background, theory, and calculations associated with VAM, Hodges [10] can be referred. VAM has been successfully applied to helicopter rotor blades [11] as they are applicable to beam like structures, where $a \ll l$ and $a \ll R$, where a is the characteristic cross-sectional dimension, l is the wavelength of deformation, and R is the radius of curvature/twist [9]. The discussion that follows is the summary of VAM and have been compiled from Ref. [10, 12, 13].

Figure 3 shows the overall flowchart describing the beam modeling process using VAM. The main idea of VAM is to decouple the 3-D problem into linear two dimensional cross-sectional analysis and a nonlinear one dimensional beam analysis. For the 2-D analysis, the cross-sectional geometry, elastic constants, and density are required. The loads and boundary conditions are supplied to the 1-D analysis. Initial twist and curvature must be supplied to both analyses. The 2-D analysis results in the cross-sectional elastic and inertia constants that can be used on the 1-D analysis. In addition, it also provides recovery relations on warping and strains to be later used. The 1-D beam analysis results in 1-D displacements, strains, and stresses. The recovery relations can then be used to recover the 3-D fields of interest.

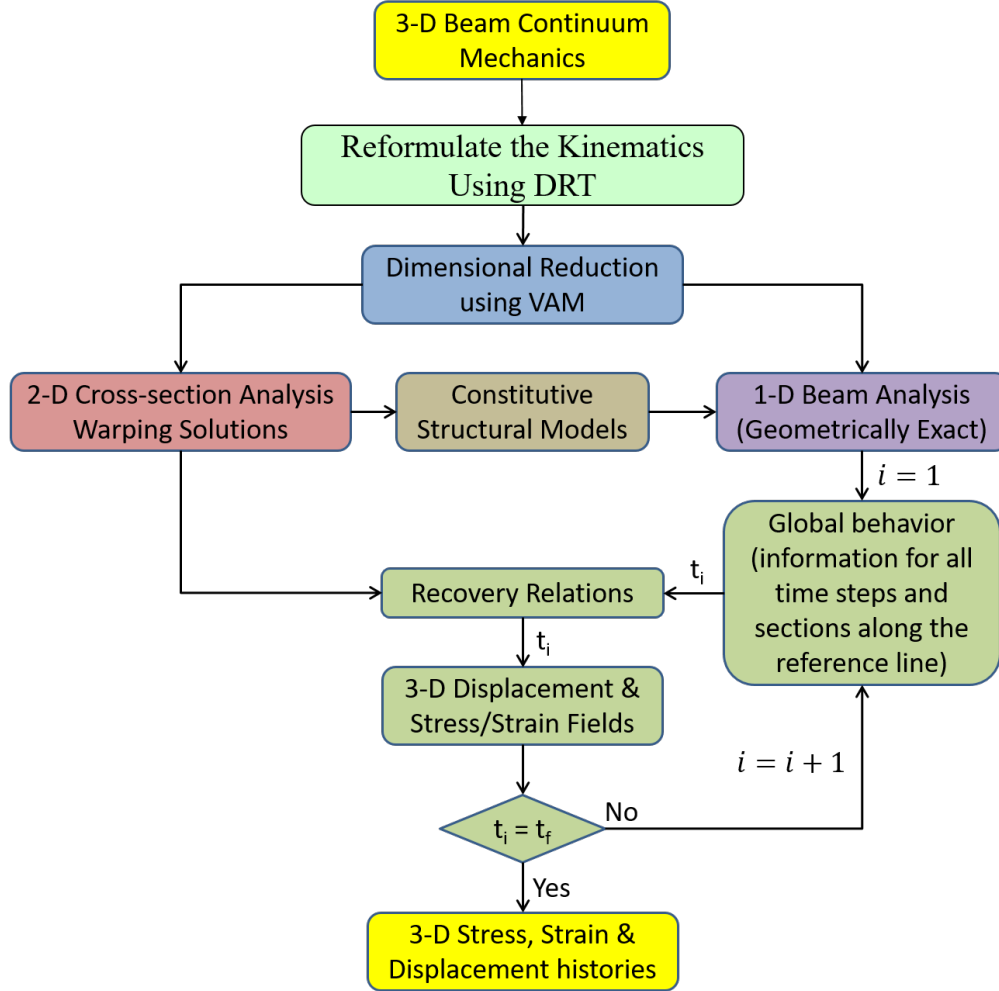


Fig. 3 Flowchart representing the structural analysis employing VAM [10].

Variational Asymptotic Beam Section (VABS) [12] and Geometrically Exact Beam Theory (GEBT) [14] are two efficient tools for 2-D cross-sectional analysis and 1-D beam analysis respectively. VAM employs asymptotic expansion of the energy functional (instead of a system of differential equations [15–17]) in terms of the small parameters (a, l, R) and makes the modeling more compact and variationally consistent; i.e. all variables follow naturally from a minimization problem based on the variational principle.

Some recent advancements to the cross-sectional analysis with regards to taper and cross-sectional obliqueness have been made by Rajagopal [18]. A comprehensive validation study for a VAM-based beam analysis against 3-D FEM for rotor blade structures is presented by Chen [19] and for thin-walled beams by Gupta et al. [20]. Further developments by Gupta et al. to expand the scope led to a framework for analysis of aperiodic and inhomogeneous beams [21]. As far as developments in GEBT are concerned, substantial improvements have been made by Wang [22] and Hodges et al. [23] by using advanced rotation parameters and implementing capability to understand the mechanical behavior of multi-functional materials, respectively.

In this paper, the tools developed from equations presented in two references [12] and [14] Viz., VABS and GEBT, respectively, are being used to solve the equivalent beam model or the intermediate beam problems generated during formulation of the equivalence model. The entire 3-D analysis for any beam problem is split into a 2-D cross-sectional analysis and a 1-D beam analysis. Here, the two subsections below lay out an overview for each of the two parts of the analysis.

A. cross-sectional Analysis using VABS

The behavior of beams is governed by the extended Hamilton's Principle as shown

$$\int_{t_1}^{t_2} [\delta(\mathcal{K} - \mathcal{U}) + \delta\overline{\mathcal{W}}] dt = 0 \quad (1)$$

where t_1 and t_2 are arbitrary fixed times, \mathcal{K} is the kinetic energy, \mathcal{U} is the internal energy, δ is the Lagrangian variation for a fixed time, and $\delta\overline{\mathcal{W}}$ is the virtual work by applied loads.

Strain energy is now written assuming that the material is linearly elastic and thus satisfies Hooke's law

$$\sigma = \mathcal{D}\Gamma \quad (2)$$

where Γ is the 3-D strain tensor and is written as $\Gamma = [\Gamma_{11} \ 2\Gamma_{12} \ 2\Gamma_{13} \ \Gamma_{22} \ 2\Gamma_{23} \ \Gamma_{33}]^T$. Here, x_i represents the beam coordinate frame such that the unit vector x_1 points along the span of the beam and x_2, x_3 are corresponding orthogonal unit vectors for the cross section. Warping functions are assumed to be of the order of the strain with assumption of small local strains. Thus, the product of warping and 1-D generalized strains may be neglected and the 3-D strain field can be written as

$$\Gamma = \Gamma_a w + \Gamma_\epsilon \bar{\epsilon} + \Gamma_{Rw} + \Gamma_{lw}' \quad (3)$$

where Γ_a is a 6×3 matrix, sparsely populated with operators of derivatives w.r.t. cross-sectional coordinates. The symbols in Eq. 3 are further defined and derived in Ref. [10]. To do the dimensional reduction, one must rely on the inherent small parameters that are present in the structure [20]. Denoting the characteristic radius of initial curvature or twist by R , the two small geometric parameters are b/l and b/R . The strain energy functional thus formed is minimized with respect to the warping functions and the warping solutions are further perturbed to obtain asymptotically correct first- and second-order approximations of the strain energy, respectively. Through this process of dimensional reduction, neglecting higher-order contributions to the energy, and transforming the energy into a beam model of the "Generalized Timoshenko" (i.e., shear deformable) form, one obtains a 1-D constitutive law relating the 1-D generalized resultant forces on the beam cross section to the 1-D generalized strains.

$$\underbrace{\begin{pmatrix} F_1 \\ F_2 \\ F_3 \\ M_1 \\ M_2 \\ M_3 \end{pmatrix}}_S = \underbrace{\begin{bmatrix} S_{11} & S_{12} & S_{13} & S_{14} & S_{15} & S_{16} \\ S_{21} & S_{22} & S_{23} & S_{24} & S_{25} & S_{26} \\ S_{31} & S_{32} & S_{33} & S_{34} & S_{35} & S_{36} \\ S_{41} & S_{42} & S_{43} & S_{44} & S_{45} & S_{46} \\ S_{51} & S_{52} & S_{53} & S_{54} & S_{55} & S_{56} \\ S_{61} & S_{62} & S_{63} & S_{64} & S_{65} & S_{66} \end{bmatrix}}_S \begin{pmatrix} \gamma_{11} \\ 2\gamma_{12} \\ 2\gamma_{13} \\ \kappa_1 \\ \kappa_2 \\ \kappa_3 \end{pmatrix} \quad (4)$$

This equation can be written in a condensed form as

$$\begin{pmatrix} F \\ M \end{pmatrix} = \begin{bmatrix} A & B \\ B^T & D \end{bmatrix} \begin{pmatrix} \gamma \\ \kappa \end{pmatrix} \quad (5)$$

where A, B and D are sub-matrices of the stiffness matrix each of size 3×3 , $F = [F_1 \ F_2 \ F_3]^T$, $M = [M_1 \ M_2 \ M_3]^T$, $\gamma = [\gamma_{11} \ 2\gamma_{12} \ 2\gamma_{13}]^T$ and $\kappa = [\kappa_1 \ \kappa_2 \ \kappa_3]^T$ as shown. Apart from this, one also obtains the 6×6 mass-matrix ($[I]$) from the cross-sectional analysis as part of the Eq. 6 which is written as

$$\begin{pmatrix} P \\ H \end{pmatrix} = [I] \begin{pmatrix} V \\ \Omega \end{pmatrix} \quad (6)$$

B. 1-D Beam Analysis using GEBT

For the purpose of 1-D analysis, the authors use the GEBT which is based on a mixed formulation. The variational statement in Eq. 1, after substituting values for \mathcal{K} , \mathcal{U} and $\delta\overline{\mathcal{W}}$ from Ref. [14], is rewritten as a variational statement in

the mixed formulation

$$\int_{t_1}^{t_2} \int_0^l \{ (\dot{\delta q} + \tilde{\Omega} \delta q + \tilde{V} \delta \psi) P + (\dot{\delta \psi} + \tilde{\Omega} \delta \psi) H - (\delta q' + \tilde{K} \delta q + (\tilde{e}_1 + \tilde{\gamma}) \delta \psi) F - (\delta \psi' + \tilde{K} \delta \psi) M + \delta q^T f + \delta \psi^T m \} dx_1 dt = \int_0^l (\delta q^T \hat{P} + \delta \psi^T \hat{H})|_{t_1}^{t_2} dx_1 - \int_{t_1}^{t_2} (\delta q^T \hat{F} + \delta \psi^T \hat{M})|_0^l dt \quad (7)$$

To proceed, the constitutive law from Eq. 5 and the momentum-velocity relations containing the mass-matrix from Eq. 6 are required. Further, to derive the mixed formulation, the kinematic differential relations in Eq. 8 are incorporated into the variational statement 7 with the help of Lagrange multipliers and using calculus of variations.

$$u' = C^{bB}(e_1 + \gamma) - e_1 - \tilde{k}u \quad (8a)$$

$$\dot{u} = C^{bB}V - v - \tilde{\omega}u \quad (8b)$$

$$c' = Q^{-1}(\kappa + k - C^{bB}k) \quad (8c)$$

$$\dot{c} = Q^{-1}(\Omega - C^{bB})\omega \quad (8d)$$

where Q is a set of Wiener-Milenković rotation parameters defined in Ref [22]. Following Wang [22], after identifying Lagrange multipliers associated with the kinematic differential equations in 8, one obtains

$$\int_0^l \{ \delta u_a^T F_a + \delta \psi_a^T M_a + \delta u_a^T (\dot{P}_a + \tilde{\omega}_a P_a) + \delta \psi_a^T [\dot{H}_a + \tilde{\omega}_a H_a + \tilde{V}_a P_a - C^{aB}(\tilde{e}_1 + \tilde{\gamma}) F_B] - \delta F_a^T [C^{aB}(e_1 + \gamma) - C^{ab} e_1] - \delta F_a^T u_a - \delta M_a^T c_a - \delta M_a^T Q^{-1} C^{ab} \kappa + \delta P_a^T (-\dot{u}_a + V_a - v_a - \tilde{\omega}_a u_a) + \delta H_a^T (\Omega_B - \omega_B - C^{ba} Q_a \dot{c}_a) - \delta u_a^T f_a - \delta \psi_a^T m_a \} dx_1 = (\delta u_a^T \hat{F}_a + \delta \psi_a^T \hat{M}_a - \delta F_a^T \hat{u}_a - \delta M_a^T \hat{c}_a)|_0^l \quad (9)$$

The variational statement in Eq. 9 is further treated using a suitable 1-D finite element discretization. Following Ref. [14], the system of equations, thus formed is solved using Newton-Raphson method along with line search algorithm to ensure global convergence. Hence, solutions for the beam 1-D displacement variables are obtained, which are further used in Section VI for validation purposes.

The remainder of this paper is organized as follows. Section IV will describe the baseline fan blade geometry, discuss the types of loads and their magnitudes being applied, and enumerate various cases being analyzed. In Section V, we will describe the modeling considerations and setup in both VABS and GEBT and COMSOL. Section VI will present the results for each case described in Section IV and follow with the discussions for each. Finally, Section VII will summarize the findings from this study and discuss planned future work.

IV. Structural Analysis

The purpose of this work is to establish relevance of beam theory tools based on VAM such as VABS (2-D sectional analysis) followed by the use of GEBT to simulate the structural behavior of a fan blade undergoing rotation in a BLI flow field. In this work, we, the authors, acknowledge that a fan blade undergoes dynamic loads that result from non-uniform work imparted by the blades in a distorted flow field. Hence, we consider that the rotor blades would structurally demonstrate a nonlinear transient behavior which is analyzed using GEBT while the required blade's cross-sectional properties are evaluated using VABS. The goal is to first compare the results for a nonlinear transient analysis obtained from the proposed technique to those obtained from 3-D FEM for a couple of simple dynamic loading scenarios considering the computational effort needed to solve problems in 3-D FEM. Once this verification is complete, the authors demonstrate the application of resulting unsteady aerodynamic loads applied on a fan blade and obtain relevant 3-D displacements and 3-D stress resultants from the proposed use of VAM based tools. With the discussions provided in subsequent sections, we finally prove that the beam theory based tools can be used to properly simulate unsteady loads on a fan blade. Further, the beam theory-based tools would be used in an optimization framework with ease as the computational time and effort is greatly reduced.

A. Baseline Geometry

Figure 4 provides a snapshot of the 3-D fan blade model. The blade geometry used in this study was obtained using a model built on the platform of Object Oriented Turbomachinery Analysis Code (OTAC) [24]. Extensions

on the multi-meanline design approach have been made to account for circumferential asymmetry in the incoming flow [25]. The blade is formed by identifying three characteristic cross sections from OTAC. Once these sections are obtained based on an efficient flow condition, we use a variable section sweep to join the sections smoothly and create the baseline geometry of the blade for structural optimization. It is to be noted that the blade has a large twist and sharp edges that make it a complex component for dynamic structural analysis. Note that this blade has not undergone any structural analysis, so the blade is not optimized for structural integrity. But in reality, it is important to design a blade which is structurally strong to withstand desired loads. Since the objective of this work is to establish the relevance of the use of VAM based tools for structural analysis, we will only focus on the mechanical response and characteristics of the stresses obtained between VABS and GEBT and compare it to that obtained from the 3-D FEA. The authors will carry out the optimization of the structural aspects of the blade as part of the future work. The geometric, material, and design parameters of the blade are listed in Table 1.

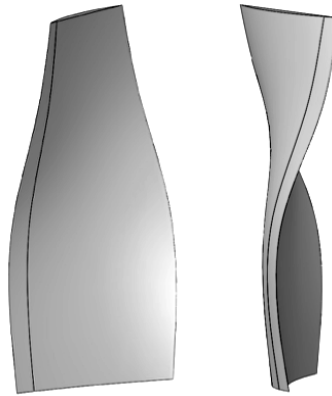


Fig. 4 3-D model of the fan blade used for analysis.

Table 1 Geometric, material, and design properties of the fan blade

Geometrical Parameters	Value	Unit	Material Properties	Value	Unit
Blade span	40	cm	Material	Titanium	-
Hub radius	16.76	cm	Young's Modulus (E)	116E09	Pa
Tip radius	55.88	cm	Poisson's ratio (ν)	0.32	-
Blade chord	20.32	cm	Density (ρ)	4506	kg/m ³
Airfoil type	DCA	-	Design Parameters	Value	Unit
Hub stagger	2.5	degrees	Design avg. mass flow	188	kg/s
Tip stagger	34.22	degrees	Design PR	1.35	-

B. Loads

In order to benchmark our studies, we will first perform analyses on loads acting on the tip of the blade – for both rotating and non-rotating cases. After verification of the results from VABS and GEBT with that of COMSOL, analysis of the rotating blade with distributed loads will be performed in VABS and GEBT to demonstrate its applicability.

1. Tip Load

Since tangential loads are more dominating for rotor blade, a sinusoidal tip transverse load is applied. Figure 5 shows the variation of this load in [0,1] seconds. The amplitude is 10,000 N with a period of 0.5s.

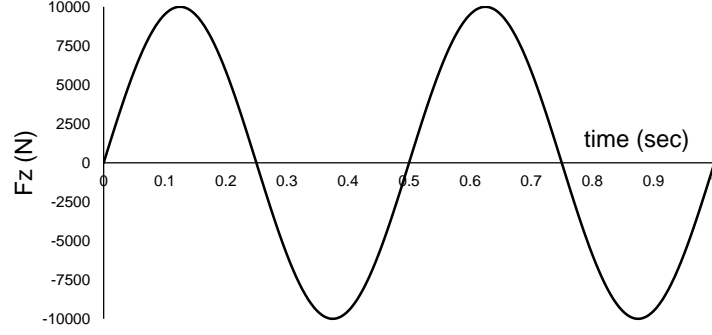


Fig. 5 Tip Loading

2. Distributed Load

The unsteady forces from the rotor performance model provides periodic excitation on the blades. As mentioned earlier, the rotor forces in this study are computed using the performance analysis through the platform of OTAC. The forces are applied as a function of time. The details of the modeling and the intermediate steps are out of the scope of this work, hence are not included in this paper. But, they can be referred in Ref. [25]. Further, the analysis considers all the geometric nonlinearities associated with the blade as well as the loading due to rotation of the fan blades.

Consider a rotor rotating at an angular velocity, ω . The rotor is shown in Figure 6 represented as a disk for simplicity. A fluid particle enters the rotor at a radius r_1 with absolute velocity V_1 , and exits the rotor at radius r_2 with absolute velocity V_2 . Here station 1 is the rotor inlet and station 2 is the rotor exit.

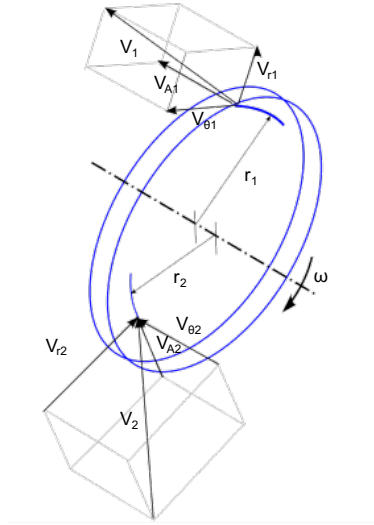


Fig. 6 A rotor represented as a wheel.

The axial force provided by the rotor is the sum of the force due to change in axial momentum and change in static pressure across the rotor. Subscript A refers to the axial property. The axial force is given by Eq. 10, where F_{AH} refers to the axial force due to momentum change and F_{AP} refers to the axial force due to pressure change.

$$F_A = F_{AH} + F_{AP} \quad (10)$$

The axial force due to momentum change through a blade passage across a rotor is given by Eq. 11, where $\Delta\dot{m}$ refers to the mass flow through the blade passage and $A_{passage}$ is the blade passage area.

$$F_{AH} = \Delta\dot{m}_1 V_{A1} - \Delta\dot{m}_2 V_{A2} = A_{passage}(\rho_1 V_{A1}^2 - \rho_2 V_{A2}^2) \quad (11)$$

The axial force due to pressure difference is given by Eq. 12

$$F_{AP} = A_{passage}(p_2 - p_1) \quad (12)$$

From Eqns. 11 and 12, Eq. 10 can be written as:

$$F_A = A_{passage}(p_2 - p_1) + A_{passage}(\rho_1 V_{A1}^2 - \rho_2 V_{A2}^2) \quad (13)$$

Similarly, the tangential force can be computed by the change in the tangential momentum of the flow across the rotor, which is given by Eq. 14, where V_θ represents the swirl velocity.

$$F_\theta = \Delta \dot{m}_1 V_{\theta 1} - \Delta \dot{m}_2 V_{\theta 2} = A_{passage}(\rho_1 V_{A1} V_{\theta 1} - \rho_2 V_{A2} V_{\theta 2}) \quad (14)$$

Since the inlet and exit flow properties are different at various locations, these forces are functions of the circumferential location (θ).

$$F_\theta, F_A = f(\theta) \quad (15)$$

Given Eq. 15 and angular frequency (ω), these forces can be converted to functions of time, as shown in Eq. 16.

$$F_\theta, F_A = f(t) \quad (16)$$

Figure 7 shows the distributed tangential and axial loads as a function of time and location of the blade presented in Figure 4. Note that since the blade's function is mostly to increase the enthalpy of the flow, the change in angular momentum is high compared to the change in axial momentum. Therefore, the tangential forces are comparatively higher in magnitude than the axial forces.

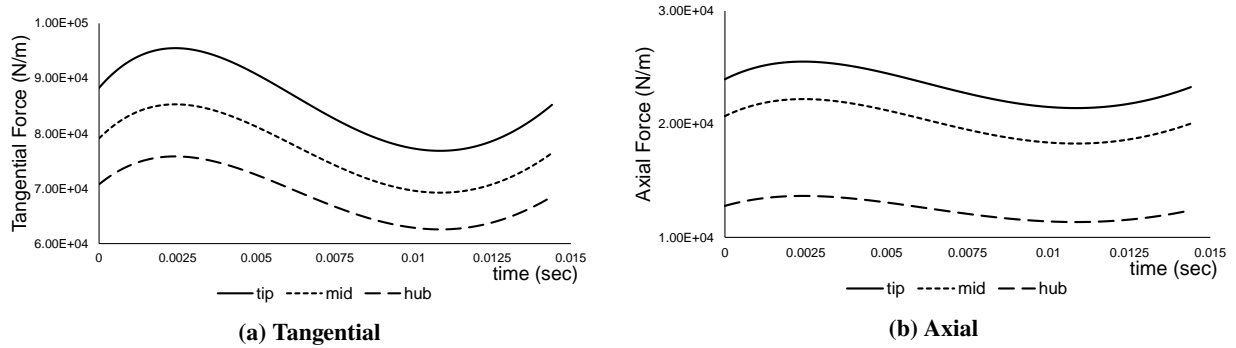


Fig. 7 Distributed Loading

C. Cases

In order to validate and demonstrate our results obtained from the beam theory based tools, VABS and GEBT, we consider four cases. The first case includes comparison of natural frequencies of the blade against those obtained from 3-D FEM. The second and third cases include comparison of displacements and stresses as a result of applying sinusoidal tip loads (with and without rotation). Finally, the fourth case includes the demonstration of VABS and GEBT to simulate the displacements and stresses for distributed loading when the blade is rotating. These cases are listed below in the order of presentation in this paper.

- 1) Eigen Analysis (non-rotating)
- 2) Tip Load (non-rotating)
- 3) Tip Load (RPM - 2500)
- 4) Distributed Load (RPM - 2500)

V. Modeling Environment

This section describes in short the modeling approaches in both beam theory based framework and 3-D FEA.

A. VABS and GEBT

As mentioned in Sec. III, completely free of ad hoc assumptions, VABS is used for 2-D cross-sectional analysis which uses the cross section of the geometry in addition to the material properties. On solving, VABS provides the 2-D sectional elastic and inertia constants in the form of 6×6 stiffness and mass matrices, respectively, if a Generalized Timoshenko model-based analysis is invoked. While the sectional stiffness matrix and the mass matrix are the primary output data from a VABS execution, the output files also include solutions to the warping variables which assist in recovery of 3-D variables once the solution of 1-D variables such as the 1-D displacements, forces, and moments are available from GEBT. Further, the information can be used to compute and visualize the stress-strain state on the cross section as well. Given a set of six section stress resultants (the axial force, the two transverse shear forces, the twisting moment, and the two transverse bending moments), which define the load acting on the section's centroid which is represented by the locus of the chosen reference line in the 1-D analysis. Further, with computation of the 3-D recovery variables using VABS, the stress distribution is obtained corresponding on a given time step at a specific cross section. This step can be repeated for all the sections to obtain values for 3-D variables for the entire 3-D geometry. Further details about the procedure and step-by-step explanation is presented by Gupta et al. [9].

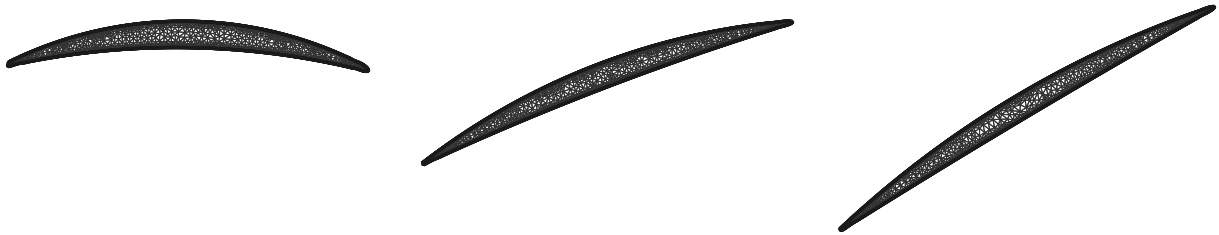


Fig. 8 Triangular mesh grid for VABS: left (hub), center (mid), right (tip)

Figure 8 shows three cross sections of the blade that were obtained from the calculations in OTAC and discretized using a very fine mesh to accommodate the intricate geometric features of the blades. Evidently, significant changes in the blade inlet and exit metal angles and twist can be observed from hub to tip. These three cross sections were required to be analyzed in VABS because these are the characteristic cross sections that define the overall blade geometry. Once these cross sections are analyzed, the required input parameters such as the initial twist, curvatures, and obliqueness, etc. for the cross section (2-D) as well as for the beam reference line (1-D) are defined in VABS and GEBT, respectively, for a correct representation of the baseline geometry for the simulation.

B. 3-D FEA using COMSOL Multiphysics

Figure 9 represents the model of the rotor blade considered for structural analysis in COMSOL. The blade is meshed using a physics-controlled fine mesh using tetrahedral elements. It is clear that the smaller regions such as the leading and trailing edges have higher mesh density as compared the bulk region of the blade. We use solid mechanics module to obtain the eigenvalues as well as the results for different time steps in a time dependent analysis. For nonlinear transient analysis as well as cases that include application of rpm on the rotor blade, we need to include geometrical nonlinearities to be able to obtain correct results as well as results which are analogous to the ones obtained from VABS and GEBT. The rpm is applied on the blade in specific cases using a rotating frame by including the centrifugal acceleration, Euler acceleration, and the spin softening. A consideration has been made to make sure that we are testing the cases in 3-D FEA which are analogous to the cases being analyzed using VAM. To enable this, we apply the tip loads over the entire cross section area with the equipotent resultant at the centroid of the cross section when compared

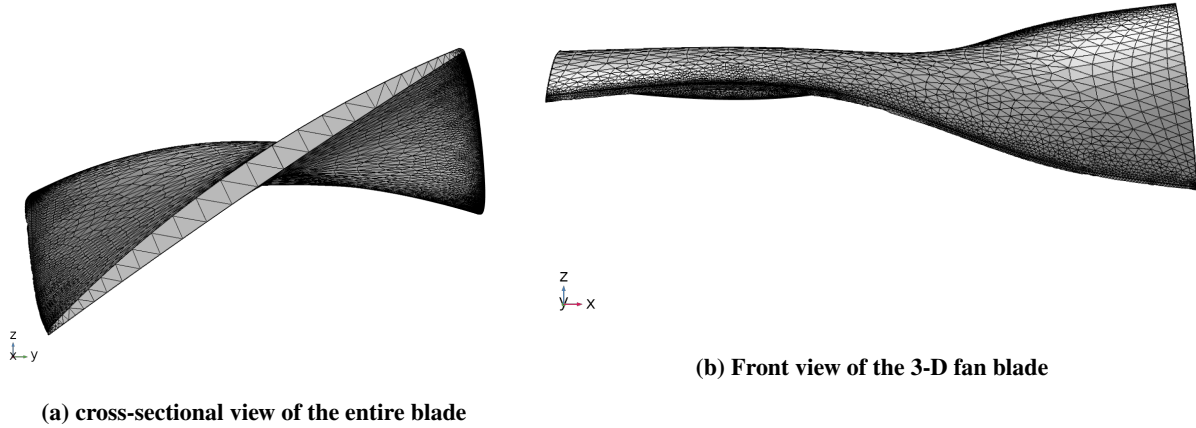


Fig. 9 Representation of the meshing of the 3-D rotor blade in COMSOL

with the analysis in VAM.

VI. Results

A. Case I: Eigenvalue Analysis (non-rotating)

For any structure undergoing dynamic loading, it is important to look at the natural frequencies of the system undergoing free vibrations. Table 2 provides a comparison of the frequencies obtained from VABS and GEBT and 3-D FEA. Mode shapes corresponding to the first 10 natural frequencies are also provided for better understanding. It is important to note that due to complex geometry of the blade, there is strong coupling between various modes such as bending in-plane and out-of-plane with torsion. It is also evident that the modes that predominantly contain contributions from torsion have eigenvalues from GEBT with significant deviation from the 3-D FEA. However, most of the eigenvalues calculated using GEBT have good agreement with the 3-D FEA with errors mentioned in the table alongside the frequencies.

B. Case II: Tip Load (non-rotating)

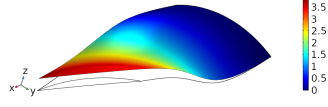
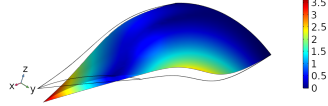
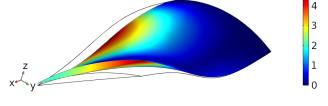
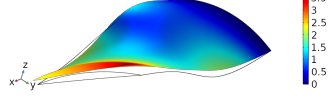
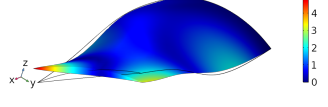
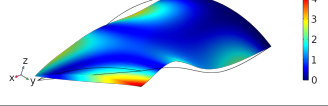
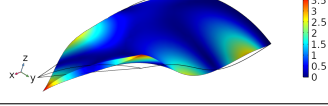
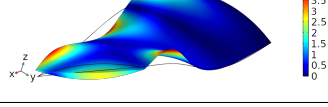
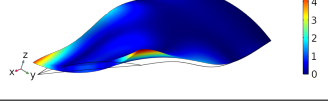
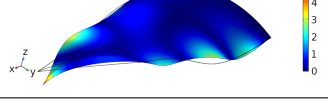
Figure 10 shows the tip displacements obtained from both VABS/GEBT and COMSOL for the sinusoidal tip load described in Sec. IV.B. The geometric and material properties of the beam are given in Table 1. We plot the dominant displacements on the cross section at the tip in y (u_2) and z (u_3) directions since the blade in x -direction (along blade's span) does not undergo any significant longitudinal displacement as compared to the out-of-plane and in-plane transverse displacements. Also, based on the frequency of the load applied (frequency of the applied load is much smaller than the fundamental frequency), the peak displacements for a cantilever beam at a given time step would be at the tip.

When the time varying sinusoidal tip load is applied, the average displacement in z -direction from COMSOL is 3.15 cm and that from VABS and GEBT is 3.07 cm (2.5% difference). It is interesting to note that the results from COMSOL show a small phase lead in the first load cycle. However, the phase difference disappears in the second load cycle (0.5 s - 1 s). This phenomenon could be observed because of a difference in the numerical damping of the two solvers considered. In the y -direction, the displacements from the two analyses do not overlap. Further investigation was not warranted in this case since the displacements in y direction is small compared to the z direction. The reason for these differences are likely attributed to the differences in the natural frequencies in the torsion mode (Table 2).

Figure 12 shows exactly how the dominant stress component σ_{11} evolve at the section present at 0.195 m in the blade along with the time stamps when the span ranges from 0.16 m to 0.6 m keeping in mind that the corresponding load values over the duration of the applied load as shown in Figure 5. Similar graphs can be obtained for the rest of the

stress components σ_{12} , σ_{13} , σ_{22} , σ_{23} and σ_{33} , but for the sake of simplicity in understanding, we resort to plotting the histories of only σ_{11} at the cross section located at a distance of 8% of the span from the root.

Table 2 Comparison of natural frequencies: VABS and GEBT vs. COMSOL

ID	Natural Frequencies (Hz)		% Difference	Mode Shape
	VABS and GEBT	COMSOL		
1	103	106	-2.83%	
2	316	361	-12.47%	
3	512	507	0.99%	
4	771	745	3.49%	
5	1171	1197	-2.17%	
6	1654	1443	14.62%	
7	1927	1872	2.94%	
8	2370	2272	4.31%	
9	2579	2726	-5.39%	
10	3076	2887	6.55%	

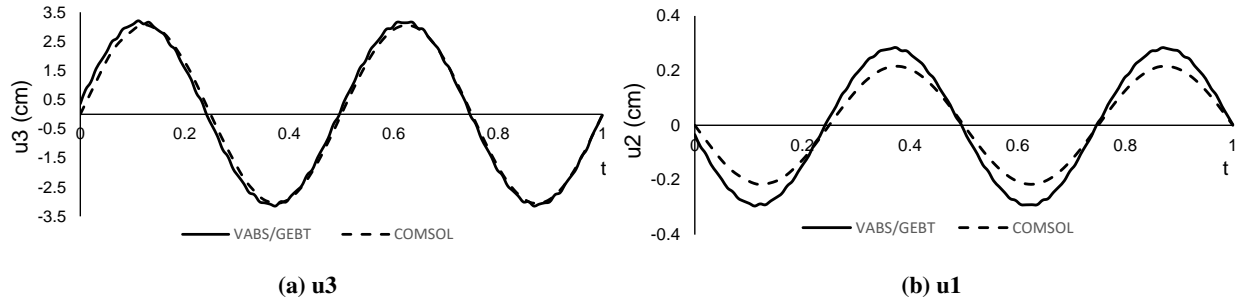


Fig. 10 Displacement at the tip (non-rotating): VABS/GEBT vs. COMSOL

Figure 11 shows the comparison of the the maximum values of σ_{11} at the desired cross section, against the results from 3-D FEA (COMSOL). Although the peak displacements match exactly between COMSOL and VABS and GEBT, the σ_{11} do not follow the same trend. The difference in peak σ_{11} obtained from VABS and GEBT and COMSOL is approximately 12%, with COMSOL predicting a lower value. We observe that the error percentage goes smaller as the time proceeds forward. Figures 11 also shows the comparison between the maximum stress locations predicted by VABS matches exactly with the ones obtained from COMSOL, and this is a really important feature when designing any new component.

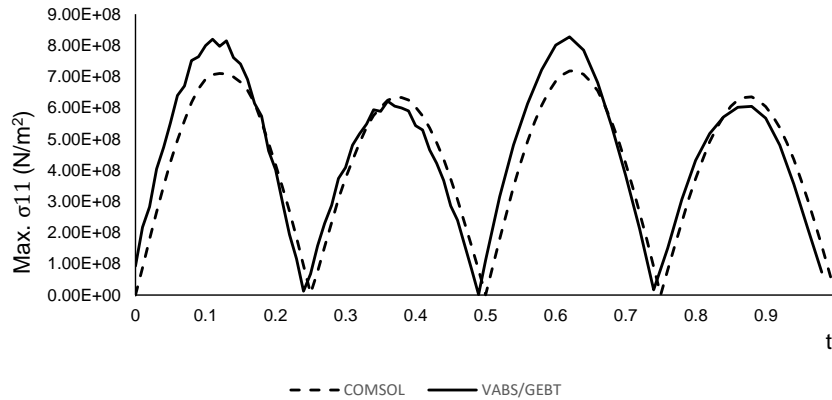


Fig. 11 Max σ_{11} at $x = 0.195m$ (non-rotating): COMSOL vs. VABS/GEBT

Similar plots for the 3-D strain variables can also be obtained through this method. Another important observation is that even though the input force is sinusoidal in nature, the output stress has a certain number of sub-peaks apart from the main peaks. This is due to the inclusion of inertia effects. It is basically due to inclusion of a higher order harmonic which will not be present if a quasi-static analysis is performed.

Table 3 shows some of the key features of the two types of approaches in determining the 3-D variables - VABS and GEBT and 3-D FEA (COMSOL). Not only does our method provide high fidelity solutions for the recovery of 3-D variables without any ad-hoc assumptions, but it is also much faster and requires minimum computational resources to achieve the same level of results as compared to a 3-D FEA software, which is our main motivation for the development of the current work. A number of important results can be extracted from the stored data depending on the requirements of the design like exact location of the maximum/minimum stress over the entire time domain, maximum displacement, 1-D force and moment variables for all time-steps, and much more.

C. Case III: Tip Load (rotating)

Figure 13 shows the displacement in the z -direction for the tip of the blade when sinusoidal load is applied as the blade is rotating (2500 RPM). As seen in the case without rotation, the displacement results from VABS and GEBT and COMSOL seem to overlap with each other. The overlapping is not as perfect as in the case without rotation. This

Table 3 Comparison of computation variables (VABS vs 3-D FEM)

Comparable	VABS + GEBT	3-D FEM (COMSOL)
Duration of Analysis	1 s	1 s
Time-Steps	100	100
Number of Elements	1000 (2-D); 400 (1-D)	1000 tet. elements/section
Memory (RAM) used	2 GB; 1-core	16 GB, 2-cores
Computation Time (Solver)	30 s (VABS) , 1 min(GEBT), 10 mins (VABS recovery w/o parallel processing) 12 mins (Total)	21.5 hrs
Storage Requirements	~ 50 MB	~ 6 GB

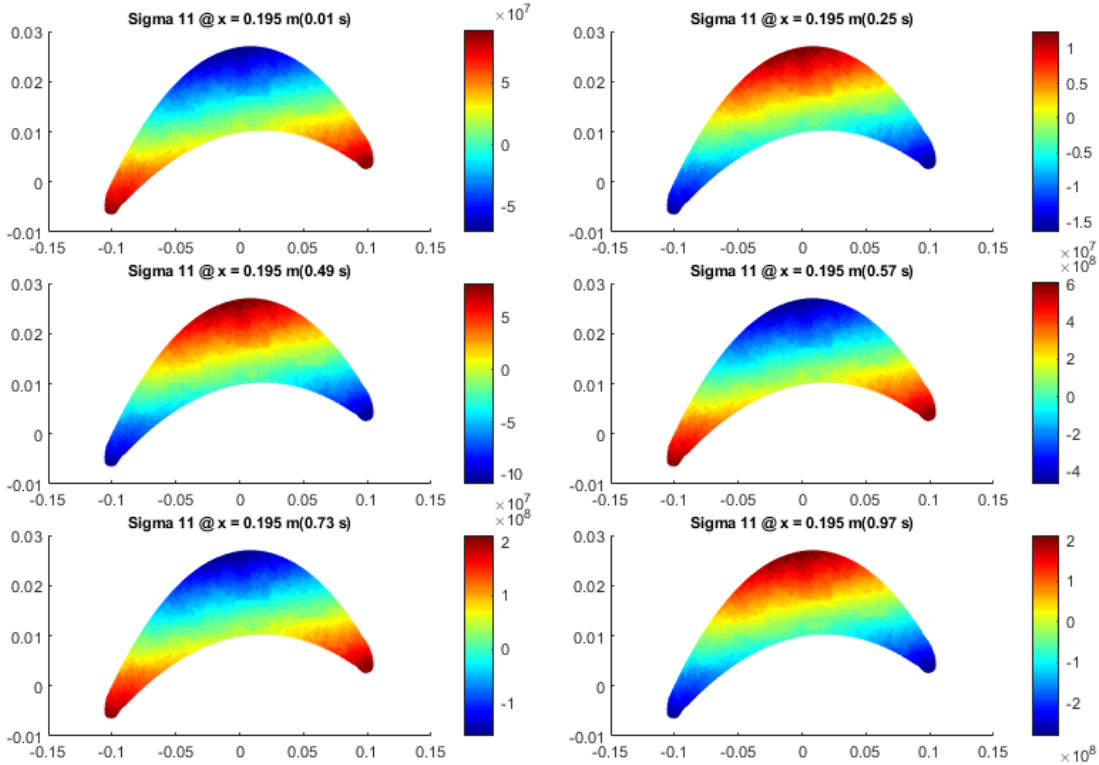


Fig. 12 σ_{11} at $x = 0.195m$ (non-rotating)

small discrepancy is mainly attributed to the fact that the results from COMSOL and VABS and GEBT were plotted for different time steps. Another observation is that the peak displacement in the $+z$ -direction is higher (approx. $+3.0$ cm) than the peak displacement in the $-z$ -direction (approx. -2.5 cm). This difference arises due to rotation. A constant rotation introduces a constant centrifugal force that offsets the non-rotating displacement curve. The third observation is the wavy nature of displacements. Upon close observation, the frequency of the waviness is almost the same in the results from both COMSOL and VABS and GEBT. This behavior is likely because of the inclusion of higher order harmonics in the response due to rotation.

Figure 14 shows the variation of maximum σ_{11} at $x = 0.195$ m at various time steps. We observed that the displacements for this case were almost close between COMSOL and VABS/GEBT. However, the solution for this case

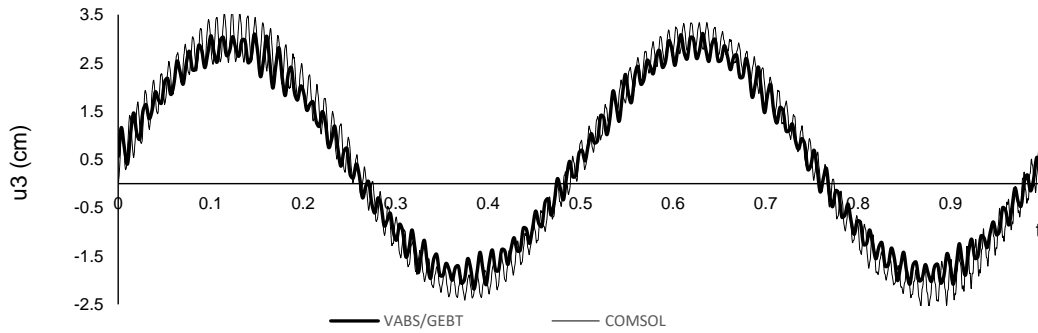


Fig. 13 Displacement at the tip (RPM - 2500)

did not converge in COMSOL when the values of maximum σ_{11} were extracted. So, only the stresses from VABS/GEBT is presented here. The plot shows two full cycles of the load being applied. Unlike the case without rotation, we do not observe similar peaks every half cycle. This is mainly again because of the rotation. As mentioned earlier, the presence of centrifugal force cause an initial displacement in the $+z$ -direction. Because of this, the stress values also show higher magnitudes in the first half cycle because of larger strains from rotation. It is also important to note that solutions from any 3-D FEA tool are highly dependent on the ability to mesh the geometry appropriately. If the geometry has sharp edges, tools such as COMSOL can not mesh the geometry appropriately and hence it affects overall convergence of the solution. An important observation we made during the analysis is that the 3-D FEA with the inclusion of geometric nonlinearities consume significantly more time and computational power to provide results when there are sharp edges involved. At times, it doesn't converge to a meaningful result at all.

Figure 15 shows exactly how the dominant stress component σ_{11} evolve at the section present at 0.195 m in the blade during rotation along with the time stamps. The corresponding load values over the duration of the applied load as shown in Figure 5.

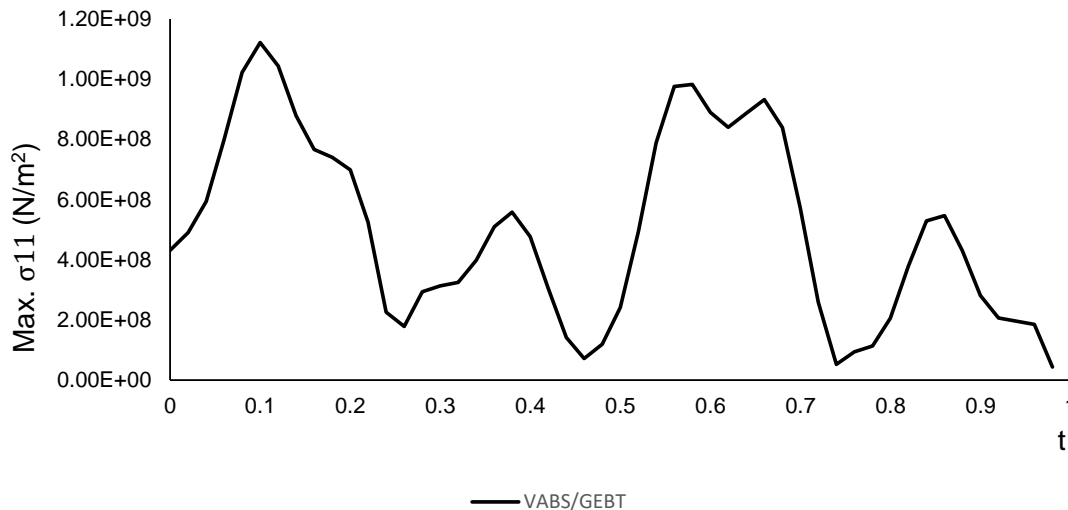


Fig. 14 Max σ_{11} at $x = 0.195m$ (RPM - 2500)

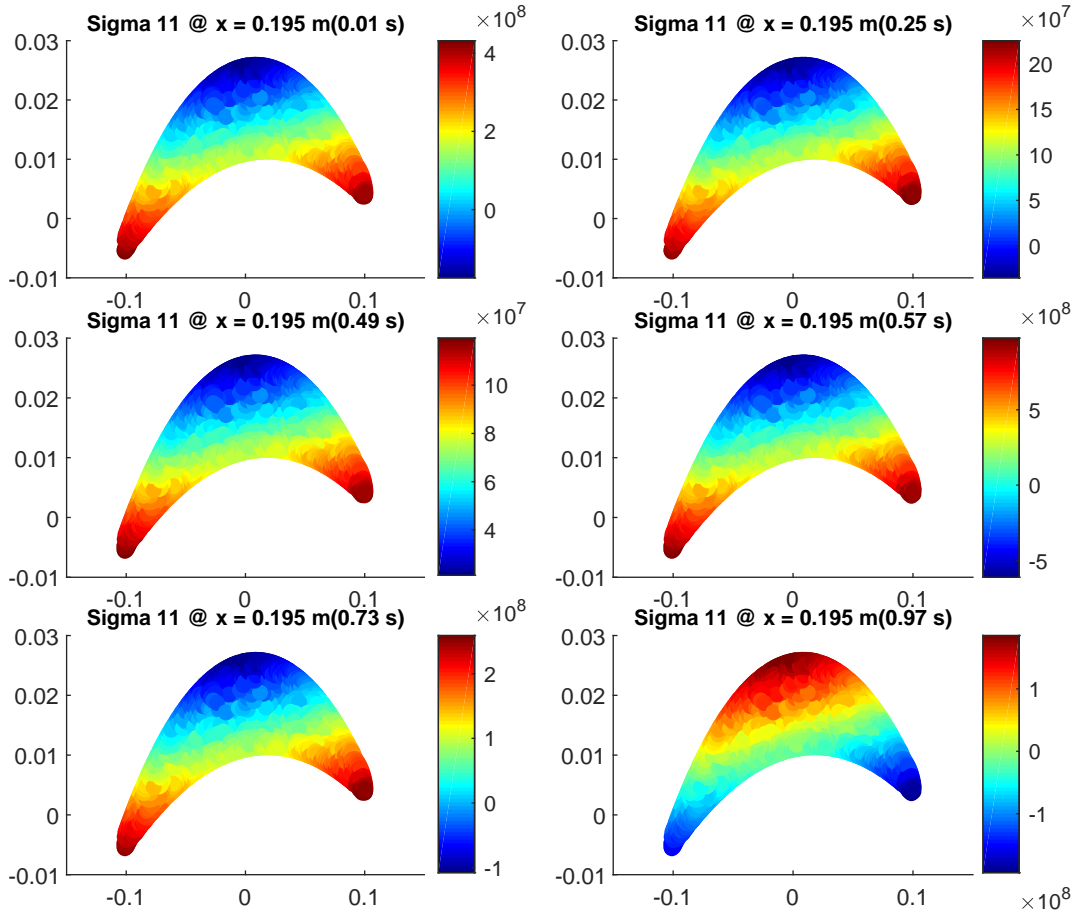


Fig. 15 σ_{11} at $x = 0.195m$ (RPM - 2500)

D. Case IV: Distributed Load (rotating)

Figure 16 shows the axial stresses near the hub ($x = 0.195 m$) and tip displacements when distributed loads are applied (as described in Sec. IV.B) as the blade is rotating (2500 RPM). In Fig. 16a, we plot the maximum value of σ_{11} at cross section represented by $x = 0.195m$ as a function of time and in Fig. 16b the average tip displacement (u_3). The displacements and stresses are plotted for two revolutions of the blade (0.048 s). We observe that the peak stresses are twice as high for distributed loads as compared to the tip sinusoidal case. The period of the plots is a result of the combination of the applied distributed loads (both axial and tangential) and the RPM. The tip sinusoidal load was just for demonstration purposes and the distributed loading was obtained from force computations from the flow properties at the inlet and the exit.

These stresses need to be compared with the stress values for criteria of failure and needs to be optimized. VABS/GEBT enable this optimization process due to their fast computational capability.

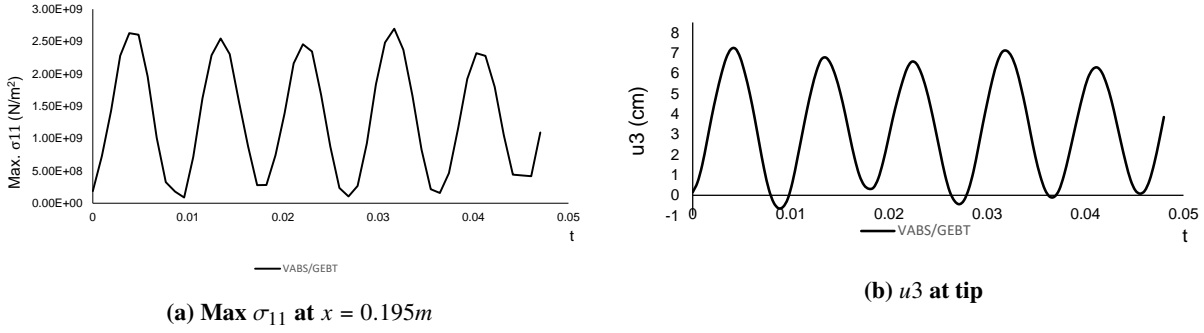


Fig. 16 Distributed Tangential and Axial Load (2500 RPM)

VII. Conclusion and Future Work

This work demonstrates the capability of VABS and GEBT to obtain 3-D stress-strain histories for fan blades undergoing rotation and dynamic loading in a nonlinear transient structural analysis. Such is the condition for the rotor blades operating in a boundary layer ingesting flow field. In the present work, we used rotating isotropic fan blade to demonstrate the results and compared them to the results obtained from 3-D FEM tool (COMSOL). It is observed that the use of VABS and GEBT for the transient structural analysis fan blades is significantly advantageous over 3-D FEM. The time required for such an analysis greatly reduces from the order of multiple hours to a few minutes. Due to the extreme fast computation times associated with VABS and GEBT, coupled with the higher fidelity of recovery relations and the ability with which complex cross sections are handled, the obtained results for the 3-D stress, strain and displacement variables are extremely accurate, fast, and require far less storage requirements when compared to COMSOL. This will no doubt provide a cutting edge tool in the conceptual design of fan blades for distortion applications, where severe structural concerns exist. In future, the authors plan to couple conceptual tools for aerodynamic design of fan blades with VAM to enable rapid investigation of aero-mechanical analysis of fan blades.

VIII. Acknowledgments

This research (contributions from Drs. Mohit Gupta and Dewey Hodges, in particular) was partially funded by the Government through the Vertical Lift Research Center of Excellence at the Georgia Institute of Technology under Agreement No. W911W6-17-2-0002. The U.S. Government is authorized to reproduce and distribute reprints for Government purposes notwithstanding any copyright notation thereon. The U.S. Government technical monitor is Mahendra Bhagwat. The Technical Points of Contact for this task are Mark V. Fulton, Louis R. Centolanza, and Hao Kang. The views and conclusions contained in this document are those of the authors and should not be interpreted as representing the official policies, either expressed or implied, of the Aviation Development Directorate or the U.S. Government.

References

- [1] Pokhrel, M., Gladin, J., Garcia, E., and Mavris, D. N., "A Methodology for Quantifying Distortion Impacts Using a Modified Parallel Compressor Theory," *ASME Turbo Expo 2018: Turbomachinery Technical Conference and Exposition*, American Society of Mechanical Engineers Digital Collection, 2018.
- [2] Pokhrel, M., Shi, M., Ahuja, J., Gladin, J., and Mavris, D. N., "Conceptual Design of a BLI Propulsor Capturing Aero-Propulsive Coupling and Distortion Impacts," *AIAA SciTech 2019 Forum*, 2019, p. 1588.
- [3] Shi, M., Pokhrel, M., Gladin, J. C., Garcia, E., and Mavris, D. N., "Modeling Fidelity Requirements of Mission-Level Analysis on Boundary Layer Ingestion Propulsion System," *AIAA Scitech 2019 Forum*, 2019, p. 1590.
- [4] Shi, M., Pokhrel, M., Gladin, J. C., Garcia, E., and Mavris, D. N., "Convergent Nozzle Gross Thrust Coefficient and Discharge Coefficient Calculation with Boundary Layer Ingestion (BLI) Effects," *53rd AIAA/SAE/ASCE Joint Propulsion Conference*, 2017, p. 5057.
- [5] Cousins, W. T., Voytovych, D., Tillman, G., and Gray, E., "Design of a Distortion-Tolerant Fan for a Boundary-Layer Ingesting Embedded Engine Application," *53rd AIAA/SAE/ASCE Joint Propulsion Conference*, 2017, p. 5042.
- [6] Campbell, W., "Protection of Turbine Disk Wheels from Axial Vibration," *Proceedings of the Cleveland Spring Meeting*, 1924.
- [7] Meher-Homji, C. B., Gabriles, G., et al., "Gas Turbine Blade Failures-Causes, Avoidance, And Troubleshooting." *Proceedings of the 27th turbomachinery symposium*, Texas A&M University. Turbomachinery Laboratories, 1998.
- [8] Berdichevskii, V., "Variational-asymptotic method of constructing a theory of shells: PMM vol. 43, no. 4, 1979, pp. 664–687," *Journal of Applied Mathematics and Mechanics*, Vol. 43, No. 4, 1979, pp. 711–736.
- [9] Gupta, M., Sarkar, K., and Hodges, D. H., "3-D Stress-Strain Histories for Composite Beams in Nonlinear Transient Structural Analysis," *AIAA Scitech 2019 Forum*, 2019, p. 1026.
- [10] Hodges, D. H., "Nonlinear Composite Beam Theory," 2006.
- [11] Yu, W., Hodges, D. H., Volovoi, V., and Cesnik, C. E., "On Timoshenko-like modeling of initially curved and twisted composite beams," *International Journal of Solids and Structures*, Vol. 39, No. 19, 2002, pp. 5101–5121.
- [12] Yu, W., Hodges, D. H., and Ho, J. C., "Variational asymptotic beam sectional analysis—an updated version," *International Journal of Engineering Science*, Vol. 59, 2012, pp. 40–64.
- [13] Gupta, M., Sarkar, K., and Hodges, D. H., "Dynamic Analysis of Nonlinear Composite Beams with 3-D Structural Damping," *AIAA Scitech 2019 Forum*, 2019, p. 0211.
- [14] Yu, W., and Blair, M., "GEBT: A general-purpose nonlinear analysis tool for composite beams," *Composite Structures*, Vol. 94, No. 9, 2012, pp. 2677–2689.
- [15] Buannic, N., and Cartraud, P., "Higher-order effective modeling of periodic heterogeneous beams. I. Asymptotic expansion method," *International Journal of Solids and Structures*, Vol. 38, No. 40-41, 2001, pp. 7139–7161.
- [16] Buannic, N., and Cartraud, P., "Higher-order effective modeling of periodic heterogeneous beams. II. Derivation of the proper boundary conditions for the interior asymptotic solution," *International Journal of Solids and Structures*, Vol. 38, No. 40-41, 2001, pp. 7163–7180.
- [17] Kim, J.-S., and Wang, K., "Vibration analysis of composite beams with end effects via the formal asymptotic method," *Journal of Vibration and Acoustics*, Vol. 132, No. 4, 2010, p. 041003.
- [18] Rajagopal, A., "Advancements in rotor blade cross-sectional analysis using the variational-asymptotic method," Ph.D. thesis, Georgia Institute of Technology, 2014.
- [19] Chen, H., Yu, W., and Capellaro, M., "A critical assessment of computer tools for calculating composite wind turbine blade properties," *Wind Energy*, Vol. 13, No. 6, 2010, pp. 497–516.
- [20] Gupta, M., and Hodges, D. H., "Modeling Thin-Walled Beams using VAM," *58th AIAA/ASCE/AHS/ASC Structures, Structural Dynamics, and Materials Conference*, 2017, p. 1832.
- [21] Gupta, M., Sarojini, D., Shah, A., and Hodges, D. H., "Dimensional Reduction Technique for Analysis of Aperiodic Inhomogeneous Structures," *2018 AIAA/ASCE/AHS/ASC Structures, Structural Dynamics, and Materials Conference*, 2018, p. 0698.

- [22] Wang, Q., and Yu, W., “Geometrically nonlinear analysis of composite beams using Wiener-Milenković parameters,” *Journal of Renewable and Sustainable Energy*, Vol. 9, No. 3, 2017, p. 033306.
- [23] Sachdeva, C., Gupta, M., and Hodges, D. H., “Modeling of initially curved and twisted smart beams using intrinsic equations,” *International Journal of Solids and Structures*, Vol. 148, 2018, pp. 3–13.
- [24] Jones, S. M., “Development of an object-oriented turbomachinery analysis code within the npss framework,” 2014.
- [25] Pokhrel, M., Gladin, J., and Mavris, D., “An Approach for Fan Stage Conceptual Design with Non-axisymmetric Stators in Presence of Distortion,” *AIAA Aviation (abstract submitted)*, 2020.